Graphene oxide ameliorates the cognitive impairment through inhibiting PI3K/Akt/mTOR pathway to induce autophagy in AD mouse model

Fangxuan Chu[1#], Kai Li[1#], Xiaolin Li[1], Lanju Xu[1], Jie Huang[2], Zhuo Yang[1*]

[1]Medical School, State Key Laboratory of Medicinal Chemical Biology, Key Laboratory of Bioactive Materials for Ministry of Education, Nankai University, Tianjin 300071, China

[2] Department of Mechanical Engineering, University College London, London, UK

Abbreviations

AD, Alzheimer's disease; Aβ, β-amyloid plaque; DEP, depotentiation; fEPSPs, field excitatory post-synaptic potentials; GO, graphene oxide; GQDs, graphene quantum dots; Hsp, heat shock proteins; IT, initial training; LC3, microtubule-associated light chain 3; LFS, low-frequency stimulation; LTP, long-term potentiation; mTOR, mammalian target of rapamycin; MWM, Morris water maze; MPP^+, 1- methyl-4-phenyl-pyridinium ion; NOR, novel object recognition; NR2B, N-methyl-d-aspartate receptor 2B; PD, Parkinson's disease; PI3K, Phosphatidylinositol-3 kinases; PSD 95, postsynaptic density protein 95; RET, reversal exploring test; RT, reversal training; SET, space exploring test; SYP, synaptophysin; SOD, Superoxide dismutase; SIRTs, Sirtuins; TEM, Transmission electron microscopy; TBS, theta burst stimulation; VaD, Vascular dementia;

Abstract: Alzheimer's disease (AD) is a neurodegenerative condition of the central nervous system characterised by cognitive impairment. Its major pathological feature is the deposition of β-amyloid (Aβ) peptide, which triggers a series of pathological cascades. Autophagy is a main pathway to eliminate abnormal aggregated proteins, and increasing autophagy represents a plausible treatment strategy against relative overproduction of neurotoxic Aβ. Graphene oxide (GO) is an emerging carbon-based nanomaterial. As a derivative of grapheme with neuroprotective effects, it can effectively increase the clearance of abnormally aggregated protein. In this article, we investigated the protective function of GO in an AD mouse model. GO (30 mg/kg, intraperitoneal) was administered for 2 weeks. The results of the Morris water maze test and the novel object recognition test suggested that GO ameliorated learning and memory impairments in 5xFAD mice. The long-term potentiation and depotentiation from the perforant path to the dentate gyrus in the hippocampus were increased with GO treatment in 5xFAD mice. Furthermore, GO upregulated the expression of synapse-related proteins and increased the cell density in the hippocampus. Our results showed that GO upregulated LC3II/LC3I and Beclin-1 and decreased p62 protein levels in 5xFAD mice. In addition, GO downregulated the PI3K/Akt/mTOR signalling pathway to induce autophagy. These results have revealed the protective potential of GO in AD.

Keywords: Graphene oxide, Alzheimer's disease, Autophagy, β-amyloid, Synaptic plasticity, Cognition.

1. Introduction

Alzheimer's disease (AD) is the most prevalent neurodegenerative condition with impaired memory and cognition. The main pathological characteristics of AD are the excessive deposition of β-amyloid (Aβ) peptide in the brain and neurofibrillary tangles due to the over-phosphorylation of tau protein, resulting in loss of neurons and synapses[1]. Progressive accumulation of Aβ can induce an inflammatory reaction, oxidative damage, neuronal cell death and disrupt synaptic signal transmission, eventually leading to cognitive dysfunction[2]. As a toxic factor, it is widely believed that excessive Aβ deposition leads to the development of AD[2, 3]. Many investigations have shown that decreased Aβ clearance is the main cause of Aβ deposition[4]. Taken together, these findings indicate that targeting Aβ is an important strategy for treating AD.

Autophagy mainly refers to macroautophagy, which is a lysosome-mediated process to maintain intracellular homeostasis and to degrade damaged organelles and misfolded/nonfunctional proteins[5]. Autophagy also plays an important role in neurodegeneration: it participates in Aβ clearance under physiological conditions and maintains Aβ homeostasis in healthy brain[6]. Recent research has shown dysfunction of the autophagy–lysosome system in AD patients[6]; impaired autophagy obstructs the ability of cells to clear Aβ, a phenomenon that leads to Aβ accumulation in the brain[7]. It seems that activating autophagy represents a promising approach to clear Aβ[6, 8]. Multiple autophagy-related proteins are required in the process of autophagy, such as microtubule-associated protein 1 light chain 3 (LC3), autophagy inducer Beclin-1 and autophagy adaptor p62 (p62)[9–11]. Mammalian target of rapamycin (mTOR) is the main regulator of autophagy and is at the centre of growth regulation. It senses a variety of environmental stimuli[12]. Abnormal mTOR signalling has been associated with many diseases, such as AD and Parkinson's disease (PD)[13]. In several studies, mTOR inhibition reduced Aβ toxicity and promoted neuron survival[4, 14–16]. The

process of Aβ-induced autophagy is also regulated by phosphoinositide 3-kinase (PI3K)/Akt/mTOR signalling[17–19]. Consequently, enhancing autophagy represents a viable approach for Aβ clearance in the brain, and it might represent a viable therapeutic target for the treatment of AD[6, 7].

Carbon-based nanomaterials have been widely used in the biomedical field because of their unique structure and biological properties[20]. Graphene oxide (GO) is a derivative of graphene – with carboxyl, hydroxyl and epoxy groups – which is widely used in biology, including for biosensing, imaging, cancer treatment, drug delivery, antibacterial activity and as a vaccine enhancer[9, 11, 21]. Compared with pristine graphene, GO has better biocompatibility, a lager specific surface area and greater stability in aqueous solution[11, 21, 22]. Nanomaterials may represent a new autophagy inducer: they can trigger autophagy effects in a variety of cell types[23]. Some nanomaterials such as ytterbium hydroxide nanorods and cerium oxide nanoparticles accelerated the removal of different forms of aggregates[24, 25]. *In vitro*, GO simultaneously destroyed the structure of Aβ and mutant huntingtin (Htt) protein aggregates (found in Huntington's disease) and enhanced the clearance rate of abnormal aggregate proteins by inducing autophagy[23, 26–28]. Furthermore, graphene induced neurite growth in a culture of pluripotent stem cells, showing neuroprotective effects[9, 29–32]. In several studies, GO induced autophagy in a variety of cells, including CT26 colon cancer cells, HeLa cells and embryonic stem cells, among others[33–35]. Therefore, the use of GO to clear abnormal aggregate proteins through inducing autophagy in the treatment of neurodegenerative diseases requires further research.

In the present study, we aimed to investigate the underlying mechanism of the GO neuroprotective effect using an AD (5xFAD) mouse model. The novel object recognition (NOR) test and Morris water maze (MWM) test were performed to assess learning and memory abilities. Subsequently, long-term potentiation (LTP) and depotentiation (DEP) from the

perforant path (PP) to the dentate gyrus (DG) were recorded to evaluate synaptic plasticity in the hippocampus. In parallel experiments, we explored a possible mechanism of action by measuring the expressions of *N*-methyl-D-aspartate receptor subunit 2B (NR2B) and postsynaptic density protein 95 (PSD-95), synaptophysin (SYP), LC3, p62, Beclin-1, P13K, AKT and mTOR. Haematoxylin and eosin (H&E) and Golgi–Cox staining were used to detect the number of neurons and density of dendritic spines in the DG. Finally, the co-localisation of LC3 and Aβ in the hippocampus was assayed by immunofluorescence staining to determine whether GO could ameliorate the synaptic plasticity impairment via enhancing autophagy levels to clear Aβ, a possible mechanism of autophagy activation in 5xFAD mouse model.

2. Materials and methods

2.1. Animals

Five-month old 5xFAD mice and wild type littermates were purchased from Nanjing BioMedical Research Institute of Nanjing University (NBRI). They were fed with a nutritionally adequate diet in the vivarium at the Medical School of Nankai University. The environment was carefully controlled in terms of temperature (23–25°C), humidity (50%–60%) and a light-dark cycle of 12 h per day. All experimental procedures followed the guidelines of the Committee for Animal Care at Nankai University, and best efforts have been made to reduce the number of experimental animals and alleviate their suffering.

Five-month-old 5xFAD mice and wild type littermates were randomly divided into four groups, each with eight mice, including four females and four males. They were: the wild type group (WT+PBS, n = 8); the wild type-treated group (WT+GO, n = 8); the 5xFAD group (AD+PBS, n = 8); and the 5xFAD-treated group (AD+GO, n = 8). The treatment was a daily 30 mg/kg body weight intraperitoneal (i.p.) injection of GO for 14 days[36], while the injection of phosphate-buffered saline (PBS) was used as a control. After treatment, a series of tests were

carried out; the experimental procedure and schedule are shown in Fig. 1A.

2.2. Preparation of GO

GO was acquired from Jiangsu XFNANO Materials Tech. Co., Ltd. The original GO nanosheet was 0.8–1.2 nm thick and 500 nm to 5 μm in diameter. GO was dispersed in sterile PBS at a concentration of 8 mg/mL, and the morphology and size of GO were observed by transmission electron microscopy (TEM) (Fig. 1B). GO appeared as a nano-monolayer translucent sheet with wrinkles and curls. The GO suspension was sonicated for 48 h (600W, 220V) below 20°C using ultrasound equipment (Ningbo Xinzhi Biological Technology Co., Ltd). After ultrasonic treatment, the morphology and size of GO were observed by TEM. The large-sized GO had broken into small-sized pieces with a 10–25 nm diameter (Fig. 1C).

2.3. Reagents

Anti-β-actin (ab179467), anti-NMDAR-2B (ab65783), anti-PSD-95 (ab18258), anti-SYP (ab32127), anti-SQSTM1/p62 (ab56416), anti-SOD1 (ab179843) and anti-SIRT1 (ab32441) were acquired from Abcam (Cambridge, UK). Anti-LC3A/B (#4108), anti-PI3K (#4255), anti-Akt (#4691), anti-phospho-Akt (#4060), anti-mTOR (#2983) and anti-phospho-mTOR (5563) were acquired from Cell Signaling Technology (Danvers, MA, United States). Anti-Beclin-1(sc-48341) was acquired from Santa Cruz Biotechnology, Inc. (Dallas, TX, United States). Anti-β-amyloid (# SIG-39142) was acquired from BioLegend (San Diego, CA, United States). The secondary antibodies of Alexa 488-conjugated goat anti-rabbit IgG, Alexa 647-conjugated goat anti-rabbit IgG and Alexa 647-conjugated goat anti-mouse IgG were acquired from Invitrogen (San Diego, CA, United States).

2.4. Behavioural tests

2.4.1. Novel object recognition (NOR) test

After 2 weeks of treatment, a series of behavioural tests were carried out. The NOR test is a behavioural assay that is commonly used to assess learning and memory[37]. The details of

the NOR process can be found in our previous study[38]. The NOR test was carried out in a silver-white box (50 × 50 × 36 cm). To prevent odour interference, 75% ethanol was used to clean the box before and in-between each run of the test.

Before starting the measurements, the mice were placed in the device for 10 min to adjust to the environment. Two identical objects (object A1, object A2) were then placed in the box to train the mice for 10 min. After 2 h, object A2 was replaced with a new object B.

In the testing phase, the mice were allowed to explore the box freely for 10 min. After 24 h, object B was replaced by another new object C, and the mice were put into the silver-white box again to explore freely for 10 min. The time the mice spent on the novel objects and the old objects were recorded automatically by a imaging system, and the recognition index was calculated as

$$\text{Recognition index} = (\text{time spent on the novel object} / \text{total contact time with new and old objects}) \times 100\%.$$

2.4.2. Morris water maze (MWM) test

The MWM test is commonly used to assess the spatial cognitive abilities in animal models[39]. After the NOR test, the mice were trained and tested in the MWM system, which includes a circular vat (diameter 90 cm, height 50 cm) and a camera that is connected to a computer to capture the swimming pathway. The water was dyed with non-toxic white dye and the temperature was maintained at $23 \pm 1°C$. A circular platform (diameter 9 cm) was placed 1–2 cm below the water surface. The north (N), south (S), east (E) and west (W) were four equal quadrants of the maze.

The MWM test included four continuous phase: initial training (IT), space exploring test (SET), reversal training (RT) and reversal exploring test (RET). The mice were trained for 5 days (once a day) with four sessions every day in the IT stage. The mice were released into the water at four different locations to find the hidden platform in the N quadrant (a maximum time

of 60 s to find the hidden platform). If a mouse was able to find the platform and stayed on it for 2–3 s, the test was completed and the mouse was taken back to the cage. If a mouse was unable to find the platform within 60 s, it was then guided to the platform and stayed on it for 20 s; the escape latency was recorded as 60s. The escape latency and swimming speed were recorded during the entire process, and the mean escape latency was used as an index of learning and memory ability.

The SET was started 24 h after the end of the IT phase. In the SET phase, the mouse was allowed to swim freely for 60 s without the platform; the dwell time on the target quadrant and the number of platform crossings during the entire process were all recorded. In the RT phase, the platform was moved to the opposite quadrant. Similar to the IT phase, the mice were trained for 3 days to find the hidden platform; the escape latency for all four groups was recorded and compared. Finally, the RET phase started 24 h after the end of the RT stage. The experimental procedure and parameters recorded were the same as those in the SET stage.

2.5. *In vivo* electrophysiological recordings

After finishing all behavioural tests, all 5xFAD mice and wild type littermates were subjected to the electrophysiological experiments to quantify the hippocampal synaptic response through field excitatory post-synaptic potentials (fEPSPs) from the PP to the DG[40, 41]. First, the mice were fixed in a stereotaxic frame (SN-3, Narishige, Japan) after they were anaesthetised with urethane (40 mg/kg body weight, i.p.). Urethane has a mild effect and can be used as a deep anaesthetic to minimise animal suffering. The animal was kept warm with a heated cotton sheet. Based on the mouse brain atlas[42], a stimulating electrode and recording electrode, respectively, were slowly positioned into the PP and the DG of the hippocampus. The PP is located 3.8 mm posterior to the bregma, 3.0 mm lateral to the midline and 1.5 mm ventral below the dura; the DG is located 2.0 mm before the bregma, 1.4 mm outside the midline and 1.5 mm ventral below the dura. The stimulative intensities (range 0.1–1 mA) were

delivered to find the best stimulation intensity that could evoke a response of 70% of its maximum slope to record a stable baseline within 30 min. After baseline, LTP in the DG was evoked by 200 Hz theta burst stimulation (TBS) consisting of 30 trains at 5 Hz of 12 pulses. Finally, DEP was evoked by low-frequency stimulation (LFS, 1 Hz, 15 min) and recorded for 60 min[43]. Clampfit 10.0 (Molecular Devices, Sunnyvale, CA, United States) was used to track the experimental data.

2.6. Western blot assay

Each group of mice was decapitated immediately after the electrophysiological experiment. The entire brain was removed from the skull and the hippocampus (n = 3 mice per group) was extracted carefully. The hippocampus was harvested and lysed on ice for 15 min in 150 mL lysis buffer. The tissue homogenate was centrifuged at 12,000 rpm and 4°C for 30 min. The protein concentration in the supernatant was quantified by the BCA method (Beyotime Biotechnology, Haimen, China). The supernatant was mixed with 5× loading buffer and boiled at 100°C for 15 min to denature the protein. Equivalent amounts of protein (30 μg) were run using sodium dodecyl sulphate–polyacrylamide gel electrophoresis (SDS–PAGE) on 8%–13% gels and then transferred onto 0.45 μm polyvinylidene difluoride (PVDF) membranes. The PVDF membranes were incubated with Tween-20 (TBST) with 5% skim milk for 1 h at room temperature to block nonspecific protein binding. Subsequently, the membranes were incubated with the primary antibodies overnight at 4°C. After washing with TBST buffer, the PVDF membranes were incubated with secondary antibodies for 50 min at room temperature. A chemiluminescence imaging system was used to image the PVDF membrane and the ImageJ program (National Institutes of Health, Bethesda, MD, United States) was used to analyse grey-scale values.

2.7. H&E staining

The brain of mice (n = 3 per group) were collected and immediately embedded in optimal

cutting temperature (OCT) at -20°C. Next, coronary slices (15 μm) were cryo-sectioned using a cryomicrotome. Sections were fixed by ethanol for 15 min and then stained with H&E. The slices were imaged using a Leica microscope (Wetzlar, Germany). These images were analysed and quantified using ImageJ to measure the number of neurons in the DG, with six sections of each sample used to calculate an average.

2.8. Golgi–Cox staining

The brain of mice (n = 3 per group) were collected and quickly immersed in a Golgi–Cox solution, following the method described previously[44], then stored for 2 weeks at room temperature (22–23°C) away from light. A refresh solution was replaced every 4–5 days during the incubation. Next, 150 μm coronary slices were acquired using a vibratome (Campden Instrument Ltd., MA752, England). The method was as follows (1) all slices were put in 6% $NaCO_3$ for 20 min at room temperature. (2) The sections were dehydrated with varying concentrations of alcohol: 70% alcohol for 10 min, 90% alcohol for 15 min, absolute alcohol I for 20 min and absolute alcohol II for 20 min. (3) All slices were transferred into xylene for 20 min for fixation and were mounted on slides with synthetic resin. The sections were then dried at room temperature and protected from light. All sections were imaged with an upright fluorescent microscope (Leica DM3000, Germany) and the spine densities of granule cells were analysed by ImageJ, with six sections of each sample used to calculate an average.

2.9. Immunofluorescence staining

The thick coronary slices (15 μm) were washed with PBS for 10 min and were permeabilised with 0.5% Triton X-100 for 15 min, followed by three 10 min washes with PBS. They were incubated with 10% normal goat serum (NGS) at room temperature for 60 min and then incubated with primary antibodies overnight at 4°C. The slices were subsequently incubated with fluorescent secondary antibody (1:1000) in the dark for 1 h at room temperature.

The nuclei were stained with 4′,6-diamidino-2-phenylindole (DAPI) for 3 min and imaged using a laser scanning confocal microscope (Olympus FV1000, Japan). Sections were analysed and quantified using ImageJ to measure the number of positive cells, with six sections of each sample used to calculate the average[45].

2.10. Data and statistical analysis

All mice in each group were randomly selected and all data were analysed with blind evaluation. GraphPad Prism 7 and SPSS 20.0 statistical software programs were used for all analyses. Data are presented as mean ± standard error of the mean (SEM). The data for escape latencies, swimming speed, number of platform crossings, target quadrant dwell time, western blot and *in vivo* electrophysiological parameters were analysed with two-way repeated measures analysis of variance (ANOVA) and the least significant difference (LSD) test for post hoc multiple comparisons. Other data were analysed by one-way ANOVA. The statistical significance was set at $p < 0.05$.

3. Results

3.1. GO improved cognitive function in 5xFAD mice

3.1.1. NOR tests

To understand the effect of GO on recognition memory abilities, the mice were tested using the NOR test, which consisted of a training phase, a short-memory testing stage (Test 1) and a long-memory testing stage (Test 2) (Fig. 2A). As shown in Fig. 2B and C, there was no significant difference in the recognition index between the objects in the training phase and Test 1 stage among the four groups ($p > 0.05$). This finding also excluded the influence of athletic ability on the experiment. As shown in Fig. 2D, the LSD test showed that the AD+PBS group had a lower recognition index compared with the WT+PBS group in the Test 2 stage (Fig. 2D, $F_{(3, 26)} = 4.552$, $p = 0.013$). Compared with the AD+PBS group, the recognition index of the AD+GO group was significantly increased in the Test 2 stage (Fig. 2D, $p = 0.024$).

However, there was no obvious difference between the WT+PBS and WT+GO groups (Fig. 2D, p = 0.665).

3.1.2. MWM test

We subsequently used the MWM test to evaluate whether GO could improve spatial cognitive function. The results for escape latency during the 5 days are shown in Fig. 3A. In the IT stage, the escape latencies were evidently decreased during the 5 days among the four groups. Compared with the WT+PBS group, the AD+PBS group spent a longer time to arrive at the platform (Fig. 3A, $F_{(3, 26)}$ = 1.853, p = 0.037 for day 1; $F_{(3, 26)}$ = 7.739, p = 0.010 for day 3; $F_{(3, 26)}$ = 3.209, p = 0.029 for day 4; $F_{(3, 26)}$ = 2.728, p = 0.035 for day 5), but not the WT+GO group (Fig. 3A, p = 0.689 on day 1; p = 0.477 on day 2; p = 0.499 on day 3; p = 0.822 on day 4; p = 0.894 on day 5). Furthermore, the AD+PBS group needed significantly longer to find the platform compared with the AD+GO group on days 3–5 (Fig. 3A, p = 0.010 for day 3; p = 0.011 for day 4; p = 0.044 for day 5). In addition, the swimming speeds did not differ among the groups throughout the process (Fig. 3B, p > 0.05), which indicates that the exercise capacity was not affected in any group.

In the SET stage, the LSD test analysed the target quadrant dwell time and number of platform crossings (Fig. 3C and D). The quadrant dwell time and number of platform crossings were decreased in the AD+PBS group compared with the WT+PBS group (Fig. 3C, $F_{(3, 26)}$ = 2.636, p = 0.038 for dwell time; Fig. 3D, $F_{(3, 26)}$ = 2.792, p = 0.049 for platform crossings), but not in the WT+GO group (Fig. 3C and D, p > 0.05). Compared with the AD+PBS group, the target quadrant dwell time and number of platform crossings were obviously increased in the AD+GO group (Fig. 3C, p = 0.033 for dwell time; Fig. 3D, p = 0.018 for platform crossings).

In the RT stage, the escape latencies were significantly longer in the AD+PBS group than those of the WT+PBS group on days 2–3 (Fig. 3E, $F_{(3, 26)}$ = 3.155, p = 0.035 for day 2; $F_{(3, 26)}$ = 2.916, p = 0.036 for day 3). After GO treatment, the escape latencies were reduced

significantly for the AD+GO group compared with the AD+PBS group on days 2–3 (Fig. 3E, $p = 0.011$ for day 2; $p = 0.037$ for day 3), but not in the WT+GO group (Fig. 3E, $p > 0.05$). The swimming speeds among all groups were not different (Fig. 3F, $p > 0.05$).

In the RET stage, the LSD test analysed the target quadrant dwell time and number of platform crossings (Fig. 3G and H). The percentage of time in the target quadrant was not different between the AD+PBS and AD+GO groups (Fig. 3G, $F_{(3, 24)} = 4.352$, $p = 0.055$). The AD+PBS group had fewer platform crossings compared with the WT+PBS group (Fig. 3H, $F_{(3, 26)} = 3.401$, $p = 0.021$), while the AD+GO group had more platform crossings compared with the AD+PBS group (Fig. 3H, $p = 0.027$). However, there was no significant difference in the WT group (Fig. 3H $p > 0.05$).

3.2. GO enhanced synaptic plasticity in the hippocampus of 5xFAD mice

Synaptic plasticity is generally considered the molecular biological mechanism of cognitive function[46]. LTP and DEP were recorded to evaluate synaptic plasticity *in vivo* (Fig. 4A). After baseline recordings, TBS was used to induce LTP from the PP to the DG. As shown in Fig. 4B and C, the fEPSP slopes were enhanced immediately in all four groups and were recorded for 60 min. The fEPSP slopes were obviously lower in the AD+PBS compared with the WT+PBS group (Fig. 4C, $F_{(3, 57)} = 21.953$, $p < 0.001$). Besides, the fEPSP slopes were obviously increased in the AD+GO compared with the AD+PBS group (Fig. 4C, $p = 0.003$), which indicates that the impaired LTP of the AD+GO group improved compared with that of the AD+PBS group. Following LTP, LFS was carried out for 15 min to induce DEP, and DEP was recorded to assess bidirectional synaptic plasticity (Fig. 4D). After LFS stimulation, LSD analysis revealed that the fEPSP slopes of DEP were strengthened significantly in the AD+PBS compared with the WT+PBS group, while the fEPSP slopes were evidently decreased in the AD+GO compared with the AD+PBS group (Fig. 4E, $F_{(3, 57)} = 41.176$, $p < 0.001$), and the fEPSP slopes of the WT+GO group were similar to the WT+PBS group (Fig. 4E, $p > 0.05$).

3.3. Effects of GO on cognition-associated protein expression

To examine the level of GO on the expression of synapse-associated proteins, the protein expression of NR2B, SYP and PSD-95 in the hippocampus were examined using western blot (Fig. 5A). The expressions of synapse-associated proteins were obviously enhanced after treatment with GO in AD mice. The expression levels of NR2B, SYP and PSD-95 were significantly lower in the AD+PBS compared with the WT+PBS group (Fig. 5D–F, $F_{(3, 12)}$ = 13.595, p = 0.001 for NR2B; $F_{(3,12)}$ = 9.908, p = 0.001 < 0.01 for SYP; $F_{(3, 27)}$ = 47.384, p < 0.001 for PSD-95). Compared with the AD+PBS group, the expression levels of NR2B, SYP and PSD-95 were significantly upregulated in the AD+GO group (Fig. 5D, p = 0.016 for NR2B; Fig. 5E, p = 0.018 for SYP; Fig. 5F, p < 0.001 for PSD-95). Treatment with GO markedly improved the synaptic plasticity impairment of AD mice, whereas the WT group did not show these changes (Fig. 5D–F, p > 0.05). Furthermore, the results of immunofluorescence staining were the same as the western blot findings (Fig. 5B and C).

3.4. GO increased neurons and tertiary dendritic spine densities of granule cells in 5xFAD mice

The cell density in the DG was determined by H&E staining (Fig. 6A). The density of cells in the DG was remarkably enhanced after treatment with GO in AD mice, but there were no significant changes in WT mice. The density of cells in the DG was significantly less in the AD+PBS compared with the WT+PBS group (Fig. 6B, $F_{(3, 15)}$ = 37.648, p < 0.001). Compared with the AD+PBS group, the number of cells was significantly increased in the DG of the AD+GO group (Fig. 6B, p < 0.001). In addition, tertiary dendritic spine densities of granule cells in the hippocampus were examined using Golgi–Cox staining (Fig. 6C, scale bar = 10 μm). Compared with the WT+PBS group, dendritic spine densities were lower in the AD+PBS group (Fig. 6D, $F_{(3,16)}$ = 32.089, p < 0.001). After treatment with GO, the tertiary dendritic spine densities of granule cells were increased in the hippocampus of the AD+GO compared

with the AD+PBS group (Fig. 6D, p = 0.002), but there were no remarkable differences in WT mice (Fig. 6D, p = 0.23).

3.5. GO reduced the deposition of Aβ in 5xFAD mice

We further explored the underlying mechanism of the GO treatment by detecting Aβ plaque deposition in the hippocampal DG and cortical regions using immunofluorescence (Fig. 7A and B). Two-way ANOVA confirmed greater Aβ plaque deposition in the DG and cortex from the AD+PBS compared with the WT+PBS group. Indeed, there was almost no Aβ plaque in the WT+PBS group (Fig. 7C, $F_{(3, 15)}$ = 64.885, p < 0.001; Fig. 7D, $F_{(3, 14)}$ = 36.561, p < 0.001). After treatment with GO, Aβ plaque deposition apparently decreased in the DG and cortex in the AD+GO compared with the AD+PBS group (Fig. 7C, p < 0.001 for the DG; Fig. 7D, p < 0.001 for the cortex), and there were no apparent changes in WT mice. These results revealed that GO reduced Aβ deposition in the brains of AD mice, thereby improving cognitive function in AD mice.

3.6. GO enhanced the autophagy level of 5xFAD mice

To investigate the potential mechanism of the Aβ decrease, autophagy marker proteins (LC3, Beclin-1 and SQSTM1/p62) were detected in the hippocampus using western blot to measure whether GO could activate autophagy to clear Aβ (Fig. 8A). Compared with the AD+PBS group, the expression of Beclin-1 and LC3II/LC3I were significantly upregulated in the AD+GO group, and the level of p62 was statistically downregulated in the AD+GO group (Fig. 8B, $F_{(3,10)}$ = 12.715, p = 0.02 for Beclin-1; Fig. 8D, $F_{(3,16)}$ = 15.451, p = 0.019 for LC3; Fig. 8C, $F_{(3,10)}$ = 13.741, p = 0.028 for p62). In addition, Beclin-1 and LC3-II/LC3-I expression was lower and p62 expression was higher in the AD+PBS compared with the WT+PBS group, which indicates that autophagy was impaired in AD mouse model (Fig. 8B, p = 0.009; Fig. 8D, p = 0.003; Fig. 8C, p = 0.001). GO increased the expression of autophagy marker proteins in the hippocampus of 5xFAD mice, but not in WT mice (Fig. 8B–D, p > 0.05). The co-

localisation of LC3 and Aβ in the cortical region was also measured using double-immunofluorescence to determine whether GO could induce autophagy to clear Aβ (Fig. 8E). There were more green dot-like structures (LC3) and fewer red irregular-like structures (Aβ) in the AD+GO compared with the AD+PBS group (Fig. 8E). There were more red dot-like structures (Beclin-1) in the AD+GO compared with the AD+PBS group (Fig. 8F), showing that there was an increase in autophagy to clear Aβ in the AD mouse model. LC3 (green) and Beclin-1 (red) expression was lower in the AD+PBS compared with the WT+PBS group (Fig. 8E and F), showing that autophagy was dysfunctional in AD compared with WT mice.

3.7. GO inhibited the PI3K/Akt/mTOR pathway in 5xFAD mice

To understand the upstream mechanism of GO-induced autophagy in the hippocampus of 5xFAD mice, we examined upstream proteins of autophagy using western blot (Fig. 9A). The p-AKT/AKT and p-mTOR/mTOR ratios were downregulated and PI3K expression was decreased in the hippocampal tissues of the AD+GO compared with the AD+PBS group (Fig. 9B, $F_{(3,10)} = 17.698$, $p = 0.003$ for p-AKT/AKT; Fig. 9C, $F_{(3,10)} = 15.334$, $p = 0.024$ for p-mTOR/mTOR; Fig. 9D, $F_{(3,10)} = 15.562$, $p = 0.001$ for PI3K). Further, the p-AKT/AKT and p-mTOR/mTOR ratios and the PI3K expression in the AD+PBS group were higher than those in the WT+PBS group (Fig. 9B, $p < 0.001$ for p-AKT/AKT; Fig. 9C, $p = 0.009$ for p-mTOR/mTOR; Fig. 9D, $p = 0.001$ for PI3K). However, there were no significant differences in WT mice.

4. Discussion

In our previous research, we found that GO enhanced Aβ clearance by inducing autophagy of microglia and neurons *in vitro*[47], so we investigated whether GO could also ameliorate cognitive impairment by activating autophagy to clear Aβ in 5xFAD mice. Our results suggest that GO enhanced autophagy via the PI3K/Akt/mTOR signalling pathway to clear Aβ and ameliorated cognitive and synaptic plasticity impairment in 5xFAD mice.

Researchers have reported that graphene and GO could destroy the structure of Aβ, promote the clearance of Aβ and abnormally aggregate Htt, and GO also could activate autophagy *in vitro*[23, 26, 28]. Graphene quantum dots (GQDs) also improved the function of learning and memory in APP/PS1 mice[48]. Jeong et al. found that neuroprotection from GO prevented PrP(106–126)-mediated neurotoxicity, with anti-tumour and anti-oxidative actions and cell proliferation promotion[29]. These findings show that GO has a tremendous latent force in the field of biomedicine, as well as in the treatment of neurodegenerative diseases such as AD. In our study, GO also showed good effects on improving cognitive function by activating autophagy in 5xFAD mice.

We used the NOR test to clarify whether GO could ameliorate the impairment of recognition memory in 5xFAD mice[37]. Our results showed that the AD+PBS group mice had a poor perception of novel objects compared with the WT+PBS group. After treatment with GO, the object memory defects were improved in 5xFAD mice. We performed the MWM test to evaluate whether the impairments in spatial cognition in 5xFAD mice could be improved by GO[49]. The IT and SET stages in the MWM test confirmed that the spatial cognition capacity was apparently impaired in 5xFAD mice, and GO treatment effectively improved spatial learning and memory in 5xFAD mice. The results of the RT and RET stages showed that treatment with GO obviously reversed the cognitive impairment of 5xFAD mice, which was consistent with the results from other graphene family studies[48, 50]. The results indicate that the capacities of spatial learning and memory were enhanced in 5xFAD mice after treatment with GO.

LTP is one of the most important manifestations of synaptic plasticity, which is the most important molecular cell model for the study of learning and memory[45, 51, 52]. DEP is closely associated with cognitive flexibility, with the ability to reduce traces of previous memories and store new information[53]. In our study, we detected synaptic transmission from the PP to DG

in the hippocampus. LTP and DEP were dysfunctional in the AD mice, and treatment with GO significantly improved the induction of LTP and weakened the synaptic connections of DEP, thus explaining the behavioural differences we observed. The data of the standardised slope of the fEPSPs in the LTP analysis explain the difference in the RT and RET phases of the MWM, and the results on DEP support the behavioural differences in the RT and RET phases of the MWM test.

It is well-known that the activation of synaptic NMDA receptors plays a main regulatory role in inducing LTP[54]. The activation of NR2B is involved in the regulation of LTP and DEP in the hippocampus and improving synaptic plasticity[38, 53]. Furthermore, PSD-95 is closely associated with the role of the NMDA receptors and contributes to synapse formation[55, 56]. The presynaptic protein SYP is located in synaptic vesicles and plays an important role in neurotransmitters release[57, 58]. Our results showed that the expression of NR2B, PSD-95 and SYP was remarkably upregulated in the AD+GO group, which further improved synaptic plasticity. The changes in the expression of synapse-related proteins further explains the results of electrophysiology experiments and indicates that synaptic mechanisms may be critical to improve the cognitive abilities of AD mice treated with GO.

Our results also support the observation that neurons are lost and the number of neurons are reduced in 5xFAD mice[59]. After GO treatment, the number of neurons increased in the DG of AD mice. Graphene and its derivatives have cellular compatibility with a variety of cell types, and GO enhances cellular neurogenesis and markedly promotes neurite elongation[22, 31, 60]. Synaptic transmission and information integration are the main functions of dendritic spines[61]. Dendritic spines are significantly reduced and lost in mouse AD models[62, 63]. Our data revealed that the density of dendritic spines markedly increased after GO treatment in AD mice.

Amyloidosis is the main pathological change of AD; it seems to induce nerve damage[64, 65], and an imbalance in the clearance of Aβ in the brain will exacerbate dementia-like

symptoms[64–66]. Compared with the AD+PBS group, the AD+GO group had less Aβ deposition in the hippocampal and cortical regions, thus confirming the benefit of GO on clearing Aβ. The levels of soluble and insoluble $Aβ_{1-42}$ and $Aβ_{1-40}$ in the brain still needs to be clarified after GO treatment. After identifying the advantage of GO on Aβ-induced cognitive obstacles, we explored the potential mechanisms. GO effectively upregulated the expression of autophagy-related proteins LC3-II/LC3-I and Beclin-1 and decreased the level of p62 in the AD+GO group. Hence, autophagy was activated in the hippocampus of the AD+GO group. In addition, LC3 and Aβ co-localisation was enhanced in the hippocampus of the AD+GO group. Changes in these proteins indicate that the autophagy pathway plays an important role in clearing Aβ.

We also focused on the reasons why GO triggered autophagy in the AD+GO group. Researchers have revealed that mTOR pathways are crucial for the regulation of autophagy[67], the activity of mTOR is prominently regulated through the PI3K/Akt pathway and the PI3K/Akt pathway is hyperactive in patients with cognitive obstacles or AD[11, 65, 68, 69]. Heras-Sandoval et al. also found that upregulation of the PI3K/AKT/mTOR pathway is closely connected with the clearance of Aβ, synaptic loss and cognitive decline in AD[12]. Recent research has indicated that GO activates the autophagic response *in vitro* via the PI3K/Akt/mTOR pathway[11]. Our previous *in vitro* experiments also showed that GO increased Aβ clearance by inducing autophagy of microglia and neurons, which inhibited the mTOR signalling pathway to induce autophagy[47]. After GO treatment, the PI3K/Akt/mTOR pathway in 5xFAD mice was inhibited; thus, it is likely that GO induced autophagy via inhibiting the PI3K/Akt/mTOR pathway.

Previous studies have revealed graphene-based materials cause cytotoxicity, oxidative stress and mitochondrial membrane changes in human dental follicle stem cells. Of note, GO induces oxidative stress without causing damage to cell membranes and presents intriguing hormetic properties, which are involved in preconditioning based neuroprotection[70, 71].

Hormesis is a biphasic dose response that has a beneficial effect with low-dose stimulation and a harmful effect with high-dose stimulation[72, 73]. Organisms trigger the hormetic response when they are exposed to mild oxidative stress; organisms respond by a variety of pleiotropic adaptive cellular programs (such as enhanced autophagy and mitochondrial reactive oxygen species [ROS] signalling) that leads to a preconditioned state, enhancing stress resistance and cell survival in age-related diseases[73]. Calabrese et al. also found that preconditioning signals leading to cellular protection through hormesis is an important redox-dependent ageing-associated neurodegenerative/neuroprotective issue in diseases such as PD, AD, and vascular dementia[74–78]. GO induces autophagy and decreases oxidative stress in *in vivo* and *in vitro* models, including exerting neuroprotective effects in a neuronal cell model[9, 29, 47, 71]. Autophagy appears to be strongly related to the mechanism underlying hormesis in age-related diseases, such as AD and PD[73]. Besides, autophagy particularly participates in redox balance in neurodegenerative diseases[79].

Redox state imbalance may lead to accumulation of unfolded or misfolded proteins in brain cells in neurodegenerative diseases[80]. The level of oxidative stress is also elevated in neuronal cells surrounding neurofibrillary tangles and Aβ deposition in AD[81]. Calabrese et al. found that the brain combats oxidative stress by integrating the expression of vitagenes, which encode heat shock proteins, thioredoxin and sirtuin systems to maintain cellular homeostasis under stressful conditions[80, 82]. For example, SIRT1 has the ability to protect cells from oxidative stress and promote cell survival in a vitagene network, with neuroprotective effects in an AD mouse model[82–84]. Recent research has reported that small-sized GO induces autophagy, decreases oxidative stress and exerts neuroprotective effects in *in vivo* and *in vitro* models[9, 47, 71]. Autophagy may be a more potent antioxidant pathway for multiple oxidative damage mechanisms in neurodegenerative diseases, which play an antioxidant function by reducing the effects of oxidative stress[85]. SIRT1-mediated induction of autophagy plays a vital

role in neuroprotection of PD cellular models[83, 84, 86]. Hormetic dose responses may be appropriate to induce endogenous neuroprotective processes in neurodevelopmental disorders[75]. In our study, we found elevated SOD1 (antioxidant enzyme) and SIRT1 expression in the hippocampus of the AD+GO compared with the AD+PBS group (Fig. S1B and C, $F_{(3, 8)} = 8.926$, $p = 0.039$ for SOD1; $F_{(3, 8)} = 9.128$, $p = 0.048$ for SIRT1). We speculate that SIRT1-mediated autophagy can be induced by GO, and autophagy may become an antioxidant pathway in GO-treated mice. Therefore, the relationship between the preconditioning signal, hormesis, redox and the vitamin network in GO-induced autophagy in an AD mouse model is worth further study.

Although GO efficiently improves cognitive function in 5xFAD mice, it is still essential to focus on the underlying toxicity of GO (a nanomaterial). Jaworski et al. reported that GO and graphene possibly have dose- and size-dependent cytotoxicity and induce genotoxicity[87, 88]. However, treatment with small-sized and low-dose ($\leq$ 50 mg/kg) GO may be safe[36]. Our results support these findings: there was no apparent neurotoxicity and no adverse effects in WT mice receiving GO treatment under the dosage (30 mg/kg) used in our study. Whether the dose and size of GO has a further impact on ameliorating the cognitive impairment in AD mice remains to be studied. Although our previous research found that GO could enhance Aβ clearance by inducing autophagy of microglia and neurons *in vitro*[47], the types of neural cells that must be awakened to clear Aβ in AD mice – and the mechanism by which this occurs – still need to be determined.

5. Conclusion

Our results show that GO treatment improves Aβ-induced cognitive impairment in AD mice and has a neuroprotective function. These findings suggest that the underlying mechanism involves GO nanosheets triggering an autophagic response to clear Aβ (Fig. 10). Our research provides new insights into the neuroprotective effect of GO and provides a novel strategy for

treating AD.

Acknowledgments

CRediT authorship contribution statement

All authors contributed to the study conception and design. Material preparation, data collection and analysis were performed by Fangxuan Chu and Kai Li. The first draft of the manuscript was written by Fangxuan Chu. Formal analysis and investigation: Xiaolin Li; Supervision, Data curation and Software.: Lanju Xu; Conceptualization, Methodology, Writing - review and editing: Jie Huang; Conceptualization, Resources, Writing - review and editing: Zhuo Yang. All authors commented on previous versions of the manuscript. All authors read and approved the final manuscript.

Conflict of interest

The authors declare that there is no conflict of interest.

References

1. Leinenga G, Götz J (2015) Scanning ultrasound removes amyloid-β and restores memory in an Alzheimer's disease mouse model. Sci Transl Med 7(278):278ra33

2. Ittner LM, Götz J. Amyloid-β and tau--a toxic pas de deux in Alzheimer's disease. Nat Rev Neurosci. 2011;12(2):65-72.

3. Reiss AB, Arain HA, Stecker MM, Siegart NM, Kasselman LJ. Amyloid toxicity in Alzheimer's disease. Rev Neurosci. 2018;29(6):613-627.

4. Rajasekhar K, Chakrabarti M, Govindaraju T. Function and toxicity of amyloid beta and recent therapeutic interventions targeting amyloid beta in Alzheimer's disease. Chem Commun (Camb). 2015;51(70):13434-13450.

5. Paquet C et al (2018) Downregulated apoptosis and autophagy after anti-Aβ immunotherapy in Alzheimer's disease. Brain Pathol 28(5):603–610

6. Caccamo A, Majumder S, Richardson A, Strong R, Oddo S. Molecular interplay between mammalian target of rapamycin (mTOR), amyloid-beta, and Tau: effects on cognitive impairments. J Biol Chem. 2010;285(17):13107-13120.

7. Menzies FM, Fleming A, Caricasole A, et al. Autophagy and Neurodegeneration: Pathogenic Mechanisms and Therapeutic Opportunities. Neuron. 2017;93(5):1015-1034.

8. Tan CC, Yu JT, Tan MS, Jiang T, Zhu XC, Tan L. Autophagy in aging and neurodegenerative diseases: implications for pathogenesis and therapy. Neurobiol Aging. 2014;35(5):941-957.

9. Cai Z, Zhao B, Li K, et al. Mammalian target of rapamycin: a valid therapeutic target through the autophagy pathway for Alzheimer's disease? J Neurosci Res. 2012;90(6):1105-1118.

10. Li Q, Liu Y, Sun M. Autophagy and Alzheimer's Disease. Cell Mol Neurobiol. 2017;37(3):377-388.

11. Chen GY, Chen CL, Tuan HY, et al. Graphene oxide triggers toll-like receptors/autophagy responses in vitro and inhibits tumor growth in vivo. Adv Healthc Mater. 2014;3(9):1486-1495.

12. Chen GY, Meng CL, Lin KC, et al. Graphene oxide as a chemosensitizer: diverted autophagic flux, enhanced nuclear import, elevated necrosis and improved antitumor effects. Biomaterials. 2015;40:12-22.

13. Feng X, Chen L, Guo W, et al. Graphene oxide induces p62/SQSTM-dependent apoptosis through the impairment of autophagic flux and lysosomal dysfunction in PC12 cells. Acta Biomater. 2018;81:278-292.

14. Munson MJ, Ganley IG (2015) MTOR, PIK3C3, and autophagy: signaling the beginning from the end. Autophagy 11(12):2375–2376

15. Heras-Sandoval D, Pérez-Rojas JM, Hernández-Damián J, Pedraza-Chaverri J. The role of PI3K/AKT/mTOR pathway in the modulation of autophagy and the clearance of protein aggregates in neurodegeneration. Cell Signal. 2014;26(12):2694-2701.

16. Wang C, Yu JT, Miao D, Wu ZC, Tan MS, Tan L. Targeting the mTOR signaling network for Alzheimer's disease therapy. Mol Neurobiol. 2014;49(1):120-135.

17. Singh AK, Kashyap MP, Tripathi VK, Singh S, Garg G, Rizvi SI. Neuroprotection Through Rapamycin-Induced Activation of Autophagy and PI3K/Akt1/mTOR/CREB Signaling Against Amyloid-β-Induced Oxidative Stress, Synaptic/Neurotransmission Dysfunction, and Neurodegeneration in Adult Rats. Mol Neurobiol. 2017;54(8):5815-5828.

18. Caccamo A, Magrì A, Medina DX, et al. mTOR regulates tau phosphorylation and degradation: implications for Alzheimer's disease and other tauopathies. Aging Cell. 2013;12(3):370-380.

19. Zhang Z, Wang X, Zhang D, Liu Y, Li L. Geniposide-mediated protection against amyloid deposition and behavioral impairment correlates with downregulation of mTOR signaling and enhanced autophagy in a mouse model of Alzheimer's disease. Aging (Albany NY). 2019;11(2):536-548.

20. Fan S, Zhang B, Luan P, et al. PI3K/AKT/mTOR/p70S6K Pathway Is Involved in Aβ25-35-Induced Autophagy. Biomed Res Int. 2015;2015:161020.

21. O' Neill C. PI3-kinase/Akt/mTOR signaling: impaired on/off switches in aging, cognitive decline and Alzheimer's disease. Exp Gerontol. 2013;48(7):647-653.

22. Perluigi M, Pupo G, Tramutola A, et al. Neuropathological role of PI3K/Akt/mTOR axis in Down syndrome brain. Biochim Biophys Acta. 2014;1842(7):1144-1153.

23. Sun Q, Wang X, Cui C, Li J, Wang Y. Doxorubicin and anti-VEGF siRNA co-delivery via nano-graphene oxide for enhanced cancer therapy in vitro and in vivo. Int J Nanomedicine. 2018;13:3713-3728. Published 2018 Jun 27.

24. Singh DP, Herrera CE, Singh B, Singh S, Singh RK, Kumar R. Graphene oxide: An efficient material and recent approach for biotechnological and biomedical applications. Mater Sci Eng C Mater Biol Appl. 2018;86:173-197.

25. Sahni D, Jea A, Mata JA, et al. Biocompatibility of pristine graphene for neuronal interface. J Neurosurg Pediatr. 2013;11(5):575-583.

26.   Jin P, Wei P, Zhang Y, et al. Autophagy-mediated clearance of ubiquitinated mutant huntingtin by graphene oxide. Nanoscale. 2016;8(44):18740-18750.

27.   Wei PF, Zhang L, Nethi SK, et al. Accelerating the clearance of mutant huntingtin protein aggregates through autophagy induction by europium hydroxide nanorods. Biomaterials. 2014;35(3):899-907.

28.   Song W, Soo Lee S, Savini M, Popp L, Colvin VL, Segatori L. Ceria nanoparticles stabilized by organic surface coatings activate the lysosome-autophagy system and enhance autophagic clearance. ACS Nano. 2014;8(10):10328-10342.

29.   Ahmad I, Mozhi A, Yang L, et al. Graphene oxide-iron oxide nanocomposite as an inhibitor of Aβ 42 amyloid peptide aggregation. Colloids Surf B Biointerfaces. 2017;159:540-545.

30.   Mahmoudi M, Akhavan O, Ghavami M, Rezaee F, Ghiasi SM. Graphene oxide strongly inhibits amyloid beta fibrillation. Nanoscale. 2012;4(23):7322-7325.

31.   Yang Z, Ge C, Liu J, et al. Destruction of amyloid fibrils by graphene through penetration and extraction of peptides. Nanoscale. 2015;7(44):18725-18737.

32.   Jeong JK, Lee YJ, Jeong SY, Jeong S, Lee GW, Park SY. Autophagic flux induced by graphene oxide has a neuroprotective effect against human prion protein fragments. Int J Nanomedicine. 2017;12:8143-8158.

33.   Chen GY, Yang HJ, Lu CH, et al. Simultaneous induction of autophagy and toll-like receptor signaling pathways by graphene oxide. Biomaterials. 2012;33(27):6559-6569.

34   Lin KC et al (2018) Graphene oxide sensitizes cancer cells to chemotherapeutics by inducing early autophagy events, promoting nuclear trafficking and necrosis. Theranostics 8(9):2477–2487.

35.   Yuan YG, Gurunathan S (2017) Combination of graphene oxide-silver nanoparticle nanocomposites and cisplatin enhances apoptosis and autophagy in human cervical cancer cells. Int J Nanomed 12:6537–6558

36.   Wei M et al (2019) Graphene oxide nanocolloids induce autophagy-lysosome dysfunction in mouse embryonic stem cells. J Biomed Nanotechnol 15(2):340–351

37.   Yang K, Gong H, Shi X, Wan J, Zhang Y, Liu Z. In vivo biodistribution and toxicology of functionalized nano-graphene oxide in mice after oral and intraperitoneal administration. Biomaterials. 2013;34(11):2787-2795.

38.   Lueptow LM. Novel Object Recognition Test for the Investigation of Learning and Memory in Mice. J Vis Exp. 2017;(126):55718.

39.   Feng L, Gao J, Wang Y, Cheong YK, Ren G, Yang Z. Etidronate-zinc Complex Ameliorated Cognitive

and Synaptic Plasticity Impairments in 2-Vessel Occlusion Model Rats by Reducing Neuroinflammation. Neuroscience. 2018;390:206-217.

40. Bromley-Brits K, Deng Y, Song W. Morris water maze test for learning and memory deficits in Alzheimer's disease model mice. J Vis Exp. 2011;(53):2920.

41. Li Z, Hao S, Yin H, Gao J, Yang Z. Autophagy ameliorates cognitive impairment through activation of PVT1 and apoptosis in diabetes mice. Behav Brain Res. 2016;305:265-277.

42. Yu M, Zhang Y, Chen X, Zhang T. Antidepressant-like effects and possible mechanisms of amantadine on cognitive and synaptic deficits in a rat model of chronic stress. Stress. 2016;19(1):104-113.

43. Hu NW, Nicoll AJ, Zhang D, et al. mGlu5 receptors and cellular prion protein mediate amyloid-β-facilitated synaptic long-term depression in vivo. Nat Commun. 2014;5:3374.

44. Brandon EP, Zhuo M, Huang YY, et al. Hippocampal long-term depression and depotentiation are defective in mice carrying a targeted disruption of the gene encoding the RI beta subunit of cAMP-dependent protein kinase. Proc Natl Acad Sci U S A. 1995;92(19):8851-8855.

45. Gibb R, Kolb B. A method for vibratome sectioning of Golgi-Cox stained whole rat brain. J Neurosci Methods. 1998;79(1):1-4.

46. Xiao X, Xu X, Li F, Xie G, Zhang T. Anti-inflammatory treatment with β-asarone improves impairments in social interaction and cognition in MK-801 treated mice. Brain Res Bull. 2019;150:150-159.

47. Martin SJ, Grimwood PD, Morris RG. Synaptic plasticity and memory: an evaluation of the hypothesis. Annu Rev Neurosci. 2000;23:649-711.

48. Li X, Li K, Chu F, Huang J, Yang Z. Graphene oxide enhances β-amyloid clearance by inducing autophagy of microglia and neurons. Chem Biol Interact. 2020;325:109126.

49. Xiao S, Zhou D, Luan P, et al. Graphene quantum dots conjugated neuroprotective peptide improve learning and memory capability. Biomaterials. 2016;106:98-110.

50. Morris R. Developments of a water-maze procedure for studying spatial learning in the rat. J Neurosci Methods. 1984;11(1):47-60.

51. D'Hooge R, De Deyn PP. Applications of the Morris water maze in the study of learning and memory. Brain Res Brain Res Rev. 2001;36(1):60-90.

52. Morris RG. Synaptic plasticity and learning: selective impairment of learning rats and blockade of long-term potentiation in vivo by the N-methyl-D-aspartate receptor antagonist AP5. J Neurosci. 1989;9(9):3040-3057.

53. Kirkwood A, Lee HK, Bear MF. Co-regulation of long-term potentiation and experience-dependent synaptic plasticity in visual cortex by age and experience. Nature. 1995;375(6529):328-331.

54. Qi Y, Hu NW, Rowan MJ. Switching off LTP: mGlu and NMDA receptor-dependent novelty exploration-induced depotentiation in the rat hippocampus. Cereb Cortex. 2013;23(4):932-939.

55. Tong G, Malenka RC, Nicoll RA. Long-term potentiation in cultures of single hippocampal granule cells: a presynaptic form of plasticity. Neuron. 1996;16(6):1147-1157.

56. Cho KO, Hunt CA, Kennedy MB. The rat brain postsynaptic density fraction contains a homolog of the Drosophila discs-large tumor suppressor protein. Neuron. 1992;9(5):929-942.

57. Toro C, Deakin JF. NMDA receptor subunit NR1 and postsynaptic protein PSD-95 in hippocampus and orbitofrontal cortex in schizophrenia and mood disorder. Schizophr Res. 2005;80(2-3):323-330.

58. Calhoun ME, Kurth D, Phinney AL, et al. Hippocampal neuron and synaptophysin-positive bouton number in aging C57BL/6 mice. Neurobiol Aging. 1998;19(6):599-606.

59. Valtorta F, Pennuto M, Bonanomi D, Benfenati F. Synaptophysin: leading actor or walk-on role in synaptic vesicle exocytosis? Bioessays. 2004;26(4):445-453.

60. Jawhar S, Trawicka A, Jenneckens C, Bayer TA, Wirths O. Motor deficits, neuron loss, and reduced anxiety coinciding with axonal degeneration and intraneuronal Aβ aggregation in the 5XFAD mouse model of Alzheimer's disease. Neurobiol Aging. 2012;33(1):196.e29-196.e1.96E40.

61. Lee JS, Lipatov A, Ha L, et al. Graphene substrate for inducing neurite outgrowth. Biochem Biophys Res Commun. 2015;460(2):267-273.

62. Fu C, Pan S, Ma Y, Kong W, Qi Z, Yang X. Effect of electrical stimulation combined with graphene-oxide-based membranes on neural stem cell proliferation and differentiation. Artif Cells Nanomed Biotechnol. 2019;47(1):1867-1876.

63. Harris KM, Kater SB. Dendritic spines: cellular specializations imparting both stability and flexibility to synaptic function. Annu Rev Neurosci. 1994;17:341-371.

64. Manczak M, Kandimalla R, Yin X, Reddy PH. Hippocampal mutant APP and amyloid beta-induced cognitive decline, dendritic spine loss, defective autophagy, mitophagy and mitochondrial abnormalities in a mouse model of Alzheimer's disease. Hum Mol Genet. 2018;27(8):1332-1342.

65. Ishizuka Y, Hanamura K.. Drebrin in Alzheimer's Disease. Adv Exp Med Biol. 2017;1006:203-223.

66. Kirouac L, Rajic AJ, Cribbs DH, Padmanabhan J. Activation of Ras-ERK Signaling and GSK-3 by Amyloid Precursor Protein and Amyloid Beta Facilitates Neurodegeneration in Alzheimer's

Disease. eNeuro. 2017;4(2):ENEURO.0149-16.2017.

67. Wang HC, Zhang T, Kuerban B, et al. Autophagy is involved in oral rAAV/Aβ vaccine-induced Aβ clearance in APP/PS1 transgenic mice. Neurosci Bull. 2015;31(4):491-504.

68. Fan L, Qiu XX, Zhu ZY, et al. Nitazoxanide, an anti-parasitic drug, efficiently ameliorates learning and memory impairments in AD model mice. Acta Pharmacol Sin. 2019;40(10):1279-1291.

69. Li F, Ma Z, Guan Z, et al. Autophagy induction by silibinin positively contributes to its anti-metastatic capacity via AMPK/mTOR pathway in renal cell carcinoma. Int J Mol Sci. 2015;16(4):8415-8429.

70. Tramutola A, Triplett JC, Di Domenico F, et al. Alteration of mTOR signaling occurs early in the progression of Alzheimer disease (AD): analysis of brain from subjects with pre-clinical AD, amnestic mild cognitive impairment and late-stage AD. J Neurochem. 2015;133(5):739-749.

71. Wang C, Zhang X, Teng Z, Zhang T, Li Y. Downregulation of PI3K/Akt/mTOR signaling pathway in curcumin-induced autophagy in APP/PS1 double transgenic mice. Eur J Pharmacol. 2014;740:312-320

72. Olteanu D, Filip A, Socaci C, et al. Cytotoxicity assessment of graphene-based nanomaterials on human dental follicle stem cells. Colloids Surf B Biointerfaces. 2015;136:791-798.

73. Ren C, Hu X, Zhou Q. Graphene Oxide Quantum Dots Reduce Oxidative Stress and Inhibit Neurotoxicity In Vitro and In Vivo through Catalase-Like Activity and Metabolic Regulation. Adv Sci (Weinh). 2018;5(5):1700595.

74. Calabrese EJ, Calabrese V, et.al. Hormesis and Ginkgo biloba (GB): Numerous biological effects of GB are mediated via hormesis. Ageing Res Rev. 2020;101019.

75. Moore MN. Lysosomes, Autophagy, and Hormesis in Cell Physiology, Pathology, and Age-Related Disease. *Dose Response*. 2020;18(3):1559325820934227.

76. Calabrese V, Santoro A, Monti D, et al. Aging and Parkinson's Disease: Inflammaging, neuroinflammation and biological remodeling as key factors in pathogenesis. *Free Radic Biol Med*. 2018;115:80-91.

77. Calabrese V, Giordano J, Ruggieri M, et al. Hormesis, cellular stress response, and redox homeostasis in autism spectrum disorders. *J Neurosci Res*. 2016;94(12):1488-1498.

78. Calabrese V, Giordano J, Signorile A, et al. Major pathogenic mechanisms in vascular dementia: Roles of cellular stress response and hormesis in neuroprotection. *J Neurosci Res*. 2016;94(12):1588-1603.

79. Brunetti G, Di Rosa G, Scuto M, et al. Healthspan Maintenance and Prevention of Parkinson's-like Phenotypes with Hydroxytyrosol and Oleuropein Aglycone in *C. elegans*. *Int J Mol Sci*. 2020;21(7):2588.

80. Di Rosa G, Brunetti G, Scuto M, et al. Healthspan Enhancement by Olive Polyphenols in *C. elegans* Wild Type and Parkinson's Models. *Int J Mol Sci*. 2020;21(11):3893.

81. Hensley K, Harris-White ME. Redox regulation of autophagy in healthy brain and neurodegeneration. *Neurobiol Dis*. 2015;84:50-59.

82. Calabrese V, Guagliano E, Sapienza M, et al. Redox regulation of cellular stress response in aging and neurodegenerative disorders: role of vitagenes. *Neurochem Res*. 2007;32(4-5):757-773.

83. Cioffi F, Adam RHI, Broersen K. Molecular Mechanisms and Genetics of Oxidative Stress in Alzheimer's Disease. J Alzheimers Dis. 2019;72(4):981-1017.

84. Calabrese V, Cornelius C, Dinkova-Kostova AT, Calabrese EJ. Vitagenes, cellular stress response, and acetylcarnitine: relevance to hormesis. *Biofactors*. 2009;35(2):146-160.

85. Bonfili L, Cecarini V, Cuccioloni M, et al. SLAB51 Probiotic Formulation Activates SIRT1 Pathway Promoting Antioxidant and Neuroprotective Effects in an AD Mouse Model. Mol Neurobiol. 2018;55(10):7987-8000.

86. Calabrese V, Cornelius C, Leso V, et al. Oxidative stress, glutathione status, sirtuin and cellular stress response in type 2 diabetes. *Biochim Biophys Acta*. 2012;1822(5):729-736.

87. Giordano S, Darley-Usmar V, Zhang J. Autophagy as an essential cellular antioxidant pathway in neurodegenerative disease. Redox Biol. 2013;2:82-90.

88. Wu Y, Li X, Zhu JX, et al. Resveratrol-activated AMPK/SIRT1/autophagy in cellular models of Parkinson's disease. *Neurosignals*. 2011;19(3):163-174.

89. El-Yamany NA, Mohamed FF, Salaheldin TA, Tohamy AA, Abd El-Mohsen WN, Amin AS. Graphene oxide nanosheets induced genotoxicity and pulmonary injury in mice. Exp Toxicol Pathol. 2017;69(6):383-392.

90. Jaworski S, Strojny B, Sawosz E, et al. Degradation of Mitochondria and Oxidative Stress as the Main Mechanism of Toxicity of Pristine Graphene on U87 Glioblastoma Cells and Tumors and HS-5 Cells. Int J Mol Sci. 2019;20(3):650.
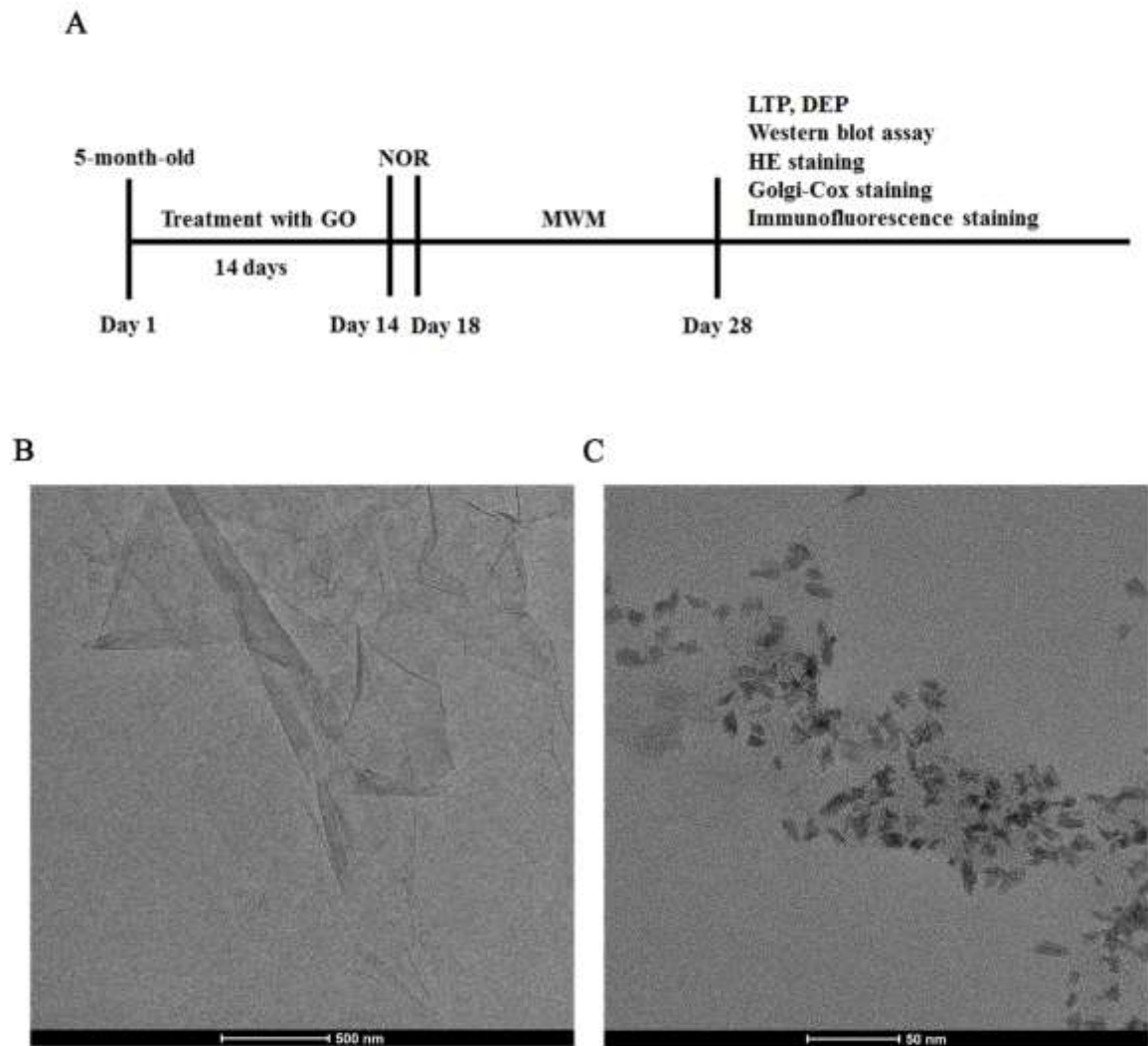
Figure 1

Fig 1 **a** The timeline of experimental design. **b** TEM of the original GO dispersion. Scale bar, 500 nm. **c** TEM of the GO after ultrasonic treatment.
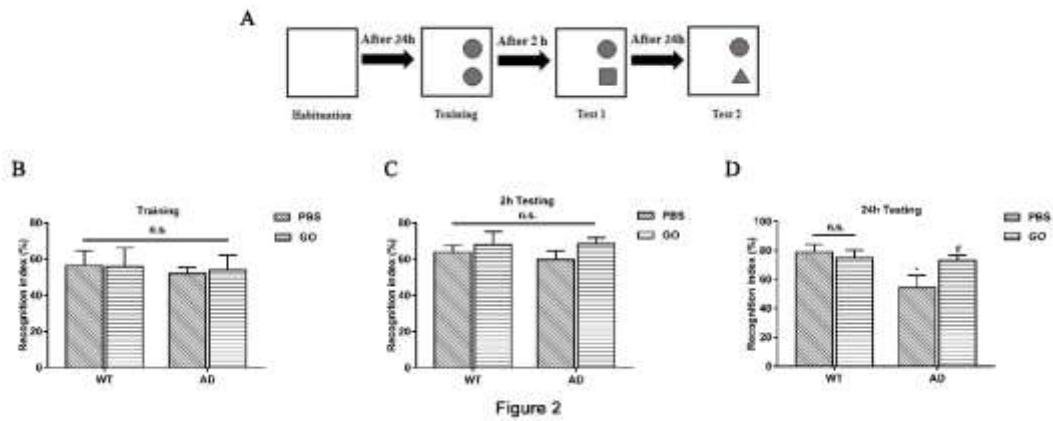
Figure 2

Fig 2 The performance of mice in NOR test. **a** The schematic of NOR test. **b** The preference in the training phase of four groups. **c** The new-object recognition index in short-memory testing phase of four groups. **d** The new-object recognition index in long-memory testing phase of four groups. Data are presented as mean $\pm$ SEM (n = 8 per group). *p < 0.05, compared with WT + PBS group; [#]p < 0.05, compared with the AD + PBS group
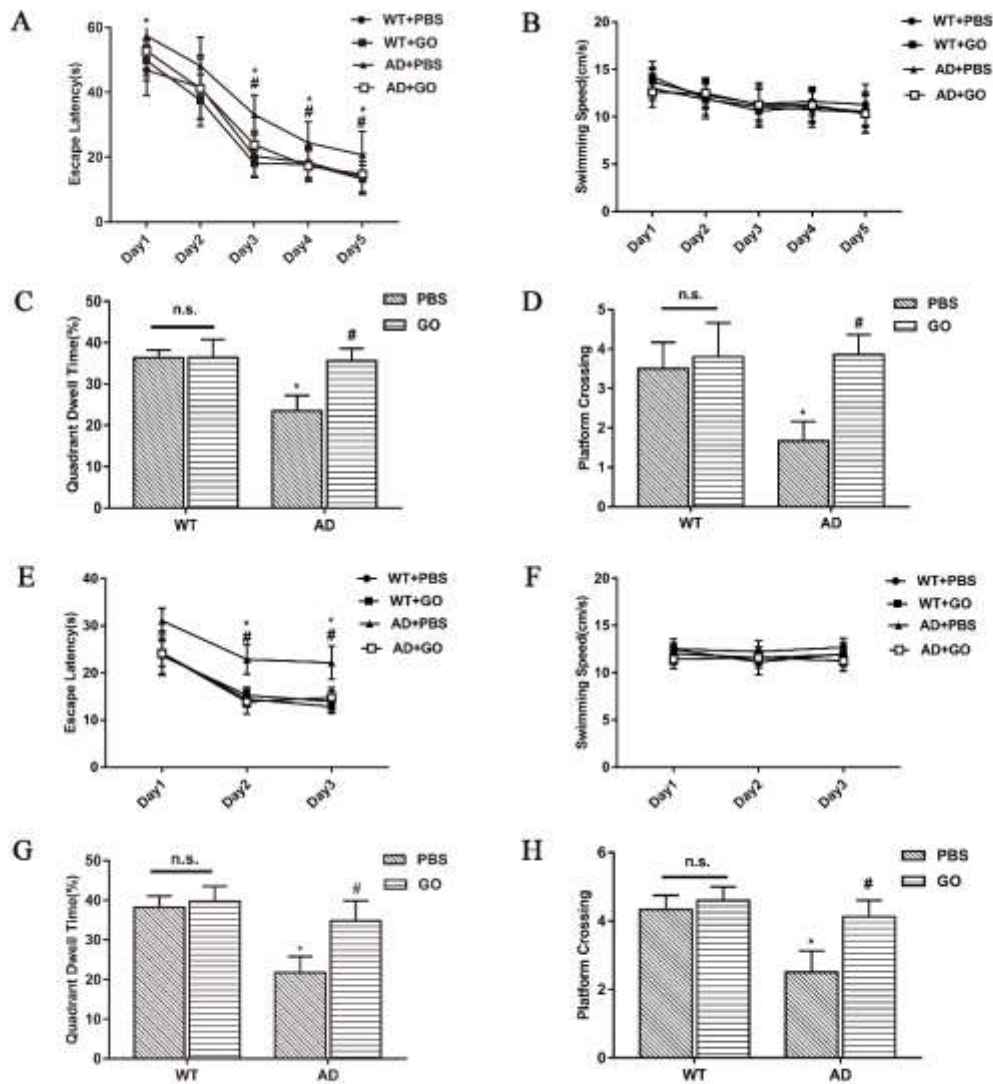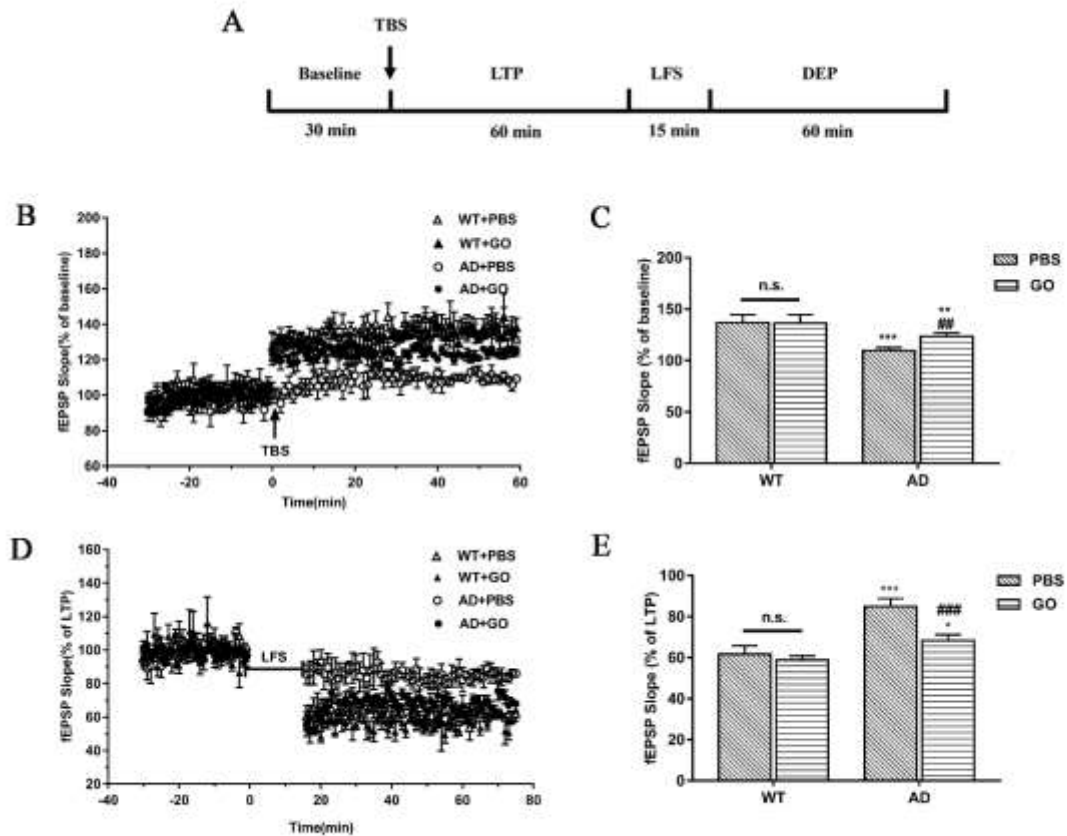
Figure 3

Fig 3 The results of MWM experiment. **a** The escape latency for 5 days in IT stage of four groups. **b** The swimming speed for 5 days in IT stage of four groups. **c** The percentage of time spent in target quadrant in the SET stage of four groups. **d** The numbers of platform crossings in SET stage of four groups. **e** The escape latency during 3 days in RT stage of four groups. **f** The swimming speed during 3 days in RT stage of four groups. **g** The percentage of time spent in target quadrant in the RET stage of four groups. **h** The numbers of platform crossings in RET stage. Data are presented as mean ± SEM (n = 8 per group). *p < 0.05 compared with WT + PBS group; #p < 0.05 compared with the AD + PBS group

Figure 4

Fig 4 Long-term potentiation (LTP) and depotentiation (DEP) from PP to DG in the hippocampus. **a** The timeline for electrophysiological recordings. **b** The changes of fEPSP slopes of LTP during four groups. The arrow represents application of a theta burst stimulation (TBS). **c** Magnitude of LTP, mean normalized fEPSP slopes between 40 and 60 min in LTP of four groups after the TBS. **d** The changes of fEPSP slopes of DEP during four groups. The arrow represents application of low-frequency stimulation (LFS). **e** Magnitude of DEP, mean normalized fEPSP slopes between 40 and 60 min in DEP of four groups after the LFS. Data are presented as mean ± SEM (n = 8 per group). *$p < 0.5$, **$p < 0.01$, ***$p < 0.001$, compared with WT + PBS group; ##$p < 0.01$, ###$p < 0.001$, compared with AD + PBS group

Figure 5
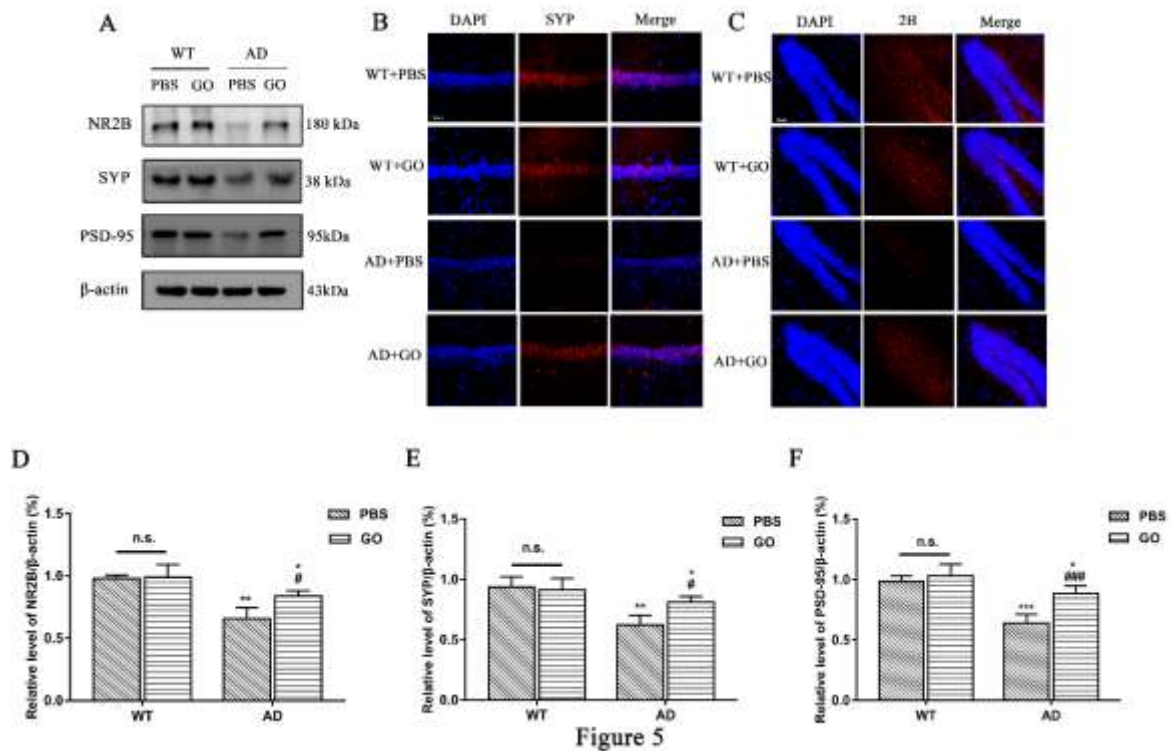
Fig 5 The expressions of NR2B, SYP and PSD-95 in the hippocampus of four groups. **a** The immunoreactive bands of NR2B (180 kDa), SYP (38 kDa), PSD-95 (85 kDa) and β-actin (43 kDa) in the hippocampal tissues. **b** The expression of SYP identified by immunofluorescence staining in the hippocampal CA1 region. Scale bar, 50 μm. **c** The expression of NR2B identified by immunofluorescence staining in the hippocampal DG region. Scale bar, 50 μm. **d** Quantitative analysis of the optical density ratio of Western blot densities of NR2B/β-actin. **e** Quantitative analysis of the optical density ratio of Western blot densities of SYP/β-actin. **f** Quantitative analysis of the optical density ratio of Western blot densities of PSD-95/β-actin. Data are presented as mean ± SEM (n = 3 per group). *p < 0.05, **p < 0.01, ***p < 0.001, compared with WT + PBS group; #p < 0.05, ###p < 0.001, compared with AD + PBS group
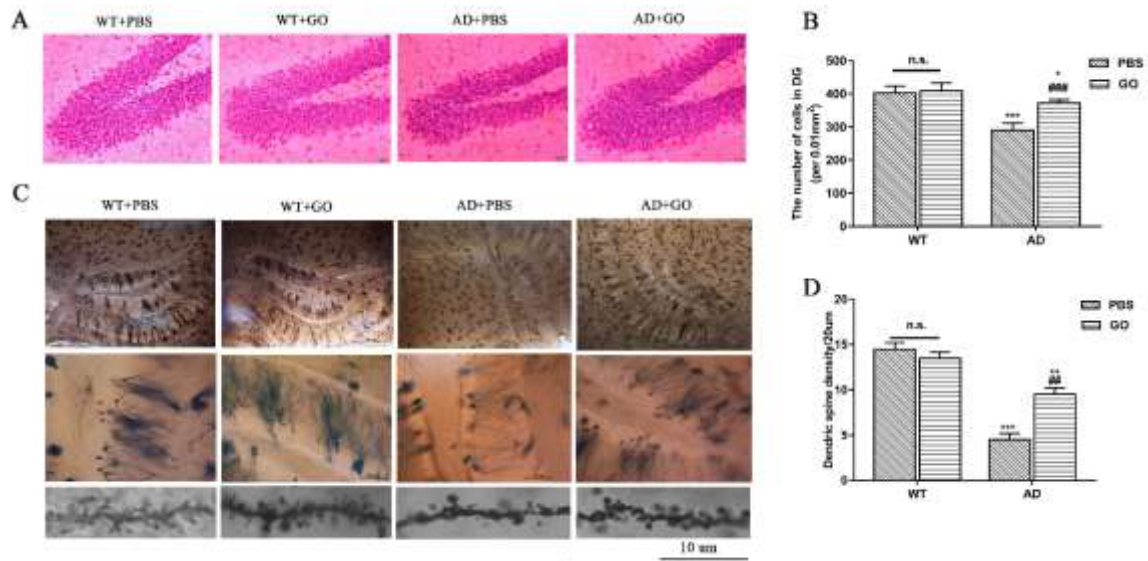
Figure 6

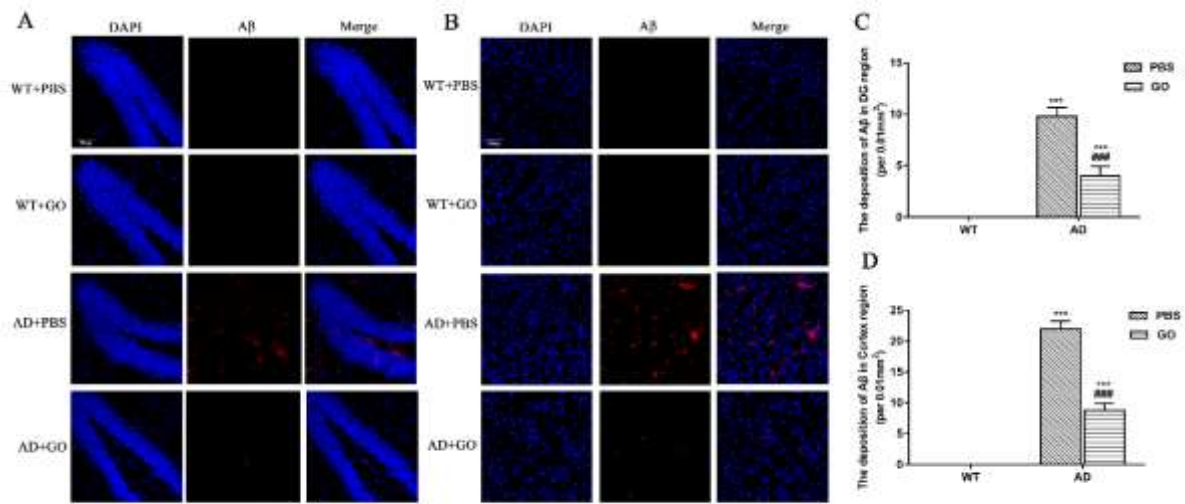Fig 6 The number of cells and the spine density in the hippocampus of the four groups. **a** Representative photomicrographs of HE staining in the hippocampal DG region of the four groups. Scale bar, 50 μm. **b** The density of DG cells of the four groups. **c** The Photomicrographs of Golgi–Cox staining in the hippocampus. Scale bar, 10 μm. **d** The density of dendritic spines in the hippocampus of WT + PBS group, WT + GO group, AD + PBS group and AD + GO group. Data are presented as mean ± SEM (n = 3 per group). *p < 0.05, **p < 0.01, ***p < 0.001, compared with WT + PBS group; ##p < 0.01, ###p < 0.001, compared with the AD + PBS group

Figure 7

Fig 7 The deposition of Aβ plaque in the hippocampal and cortical regions of the four groups.
a Representative photomicrographs of immunofluorescence staining in DG region of the four
groups. Scale bar, 50 μm. **b** Representative photomicrographs of immunofluorescence staining
in cortex region of the four groups. Scale bar, 50 μm. **c** Quantification of Aβ in DG region by
counting the deposition of Aβ plaque in the four groups. **d** Quantification of Aβ in cortex region
by counting deposition of Aβ plaque in the four groups. Data are presented as mean ± SEM
(n = 3 per group). ***p < 0.001, compared with WT + PBS group; ###p < 0.001, compared with
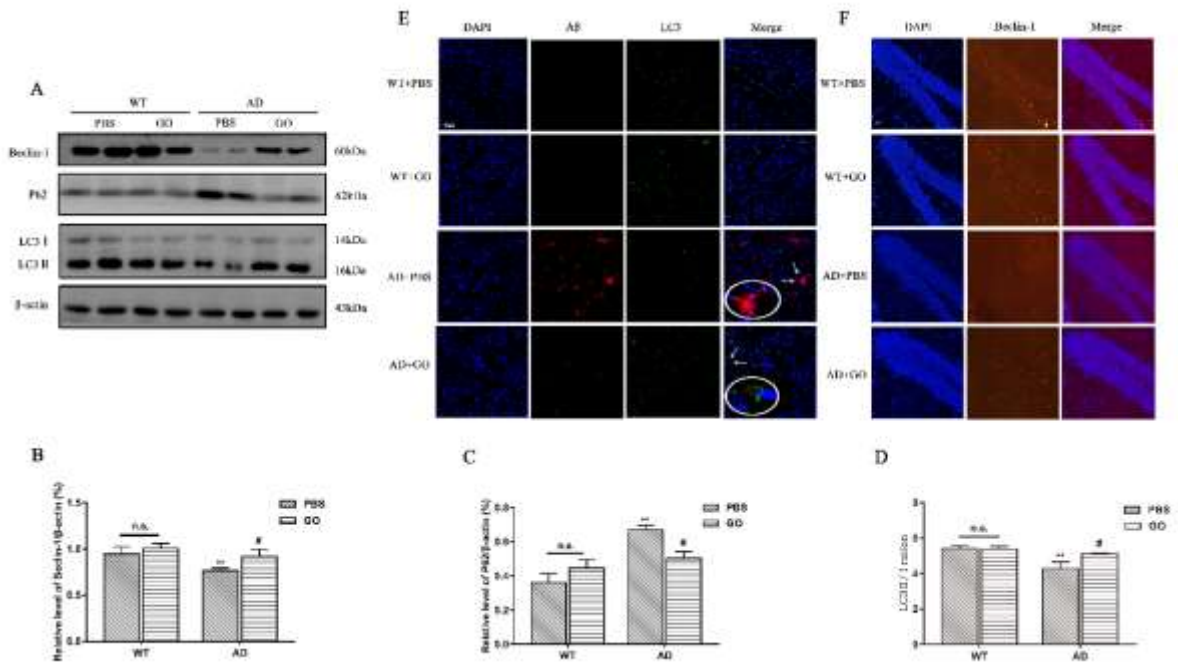the AD + PBS group

Figure 8

Fig 8 The effect of GO-induced autophagy level in the hippocampus. **a** The representative bands of western blot for Beclin-1 (60 kDa), p62 (62 kDa), LC3-I (16 kDa), LC3-II (14 kDa) and β-actin (43 kDa). **b** Quantitative analysis of western blot densities of Beclin-1. **c** Quantitative analysis of Western blot densities of p62. **d** Quantitative analysis of the LC3II-/LC3-I ratio. The expression of proteins in Western blot assay was normalized with β-actin. **e** Double-immunofluorescence using LC3 and Aβ antibodies in cortex region of the four groups. Scale bar, 50 μm. **f** The expressions of Beclin-1 identified by immunofluorescence staining in the hippocampal DG region of the four groups. Scale bar, 50 μm. Data are presented as mean ± SEM (n = 3 per group). **p < 0.01, compared with WT + PBS group; #p < 0.05, compared with the AD + PBS group
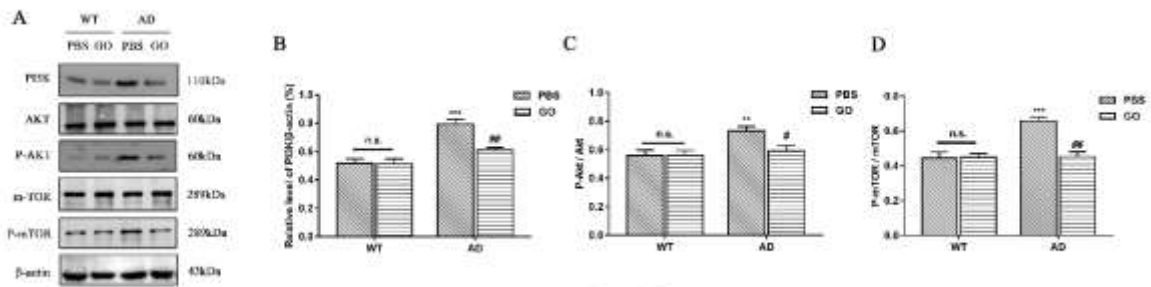
Figure 9

Fig 9 GO inhibited PI3K/Akt/mTOR pathway in the hippocampus of 5xFAD mice. **a** The representative bands of western blot assay for P13K (110 kDa), AKT (60 kDa), p-AKT (60 kDa), mTOR (289 kDa), p-mTOR (289 kDa) and β-actin (43 kDa). **b** Quantitative analysis of western blot densities of P13K. **c** Quantitative analysis of western blot densities of p-AKT/AKT ratio. **d** Quantitative analysis of the p-mTOR/mTOR ratio. The protein expressions in western blots are normalized with β-actin. Data are presented as mean ± SEM (n = 3 per group). **p < 0.01, ***p < 0.001, compared with WT + PBS group; #p < 0.05, ##p < 0.01, compared with the AD + PBS group
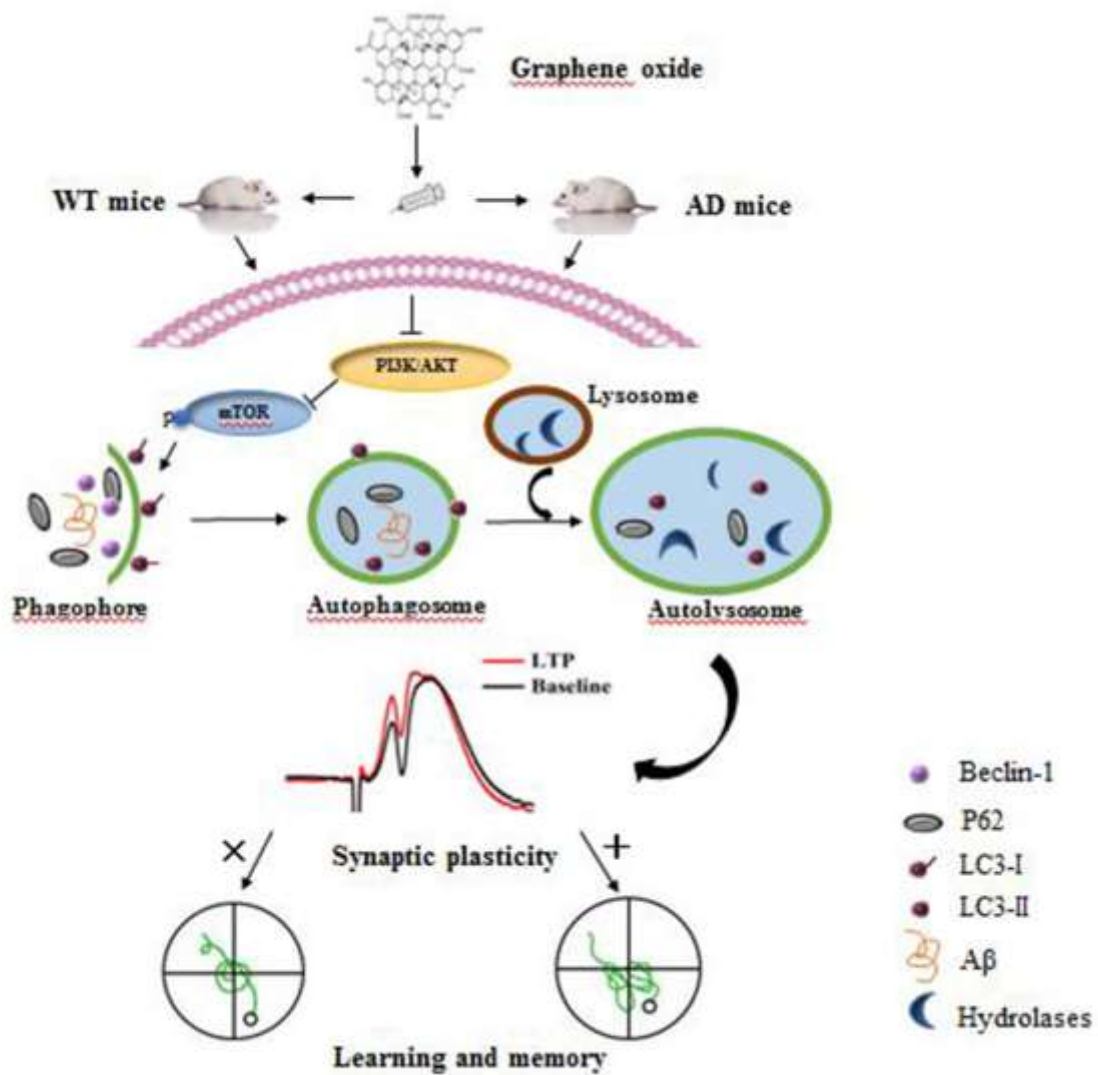
Figure 10

Fig 10 Graphical abstract illustrates the mechanism of Graphene oxide (GO) ameliorating cognitive impairment in AD model mice. We proposed that GO ameliorated Aβ-induced cognitive deficits through inhibiting PI3K/Akt/mTOR pathway to activate autophagy, and improved cognitive and synaptic plasticity function in AD model mice. Our observations support that GO could be regarded as a neuroprotective nanomaterial with efficacy in neurodegenerative diseases. The red " + " represented a great influence; the black " × " represented a rarely influence
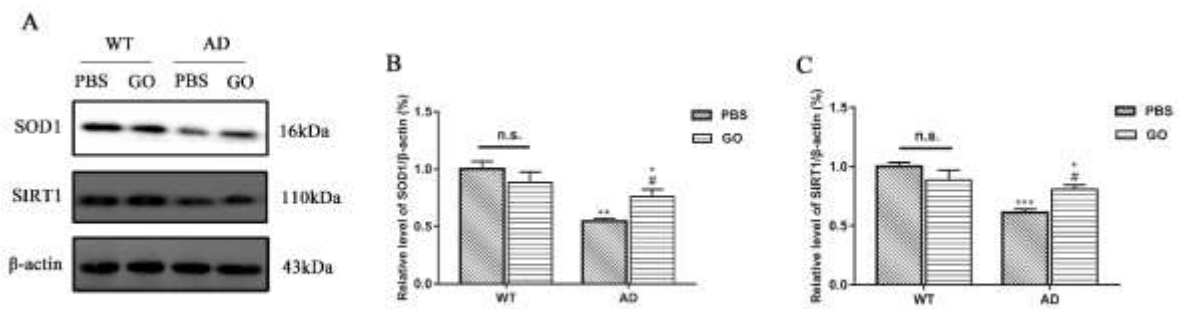
Figure S1

Fig. S1 The expressions of SOD1 and SIRT1 in the hippocampal of four groups. (A) The immunoreactive bands of SOD1 (16 kDa), SIRT1 (110 kDa) and β-actin (43 kDa) in the hippocampal tissues. (B) Quantitative analysis of the optical density ratio of western blot densities of SOD1. (C) Quantitative analysis of the optical density ratio of western blot densities of SIRT1. The expression of proteins in western blots are normalized with β-actin. Data are presented as mean ± SEM (n = 3 per group). *$p < 0.05$, **$p < 0.01$, ***$p < 0.001$, compared with WT+PBS group; #$p < 0.05$, compared with the AD+PBS group.